Inorganic Chemistry

Article

pubs.acs.org/IC

Ground-State and Excited-State Structures of Tungsten−Benzylidyne Complexes

Benjamin M. Lovaasen,[†,⊥] Jenny V. Lockard,[‡,∥] Brian W. Cohen,[†] Shujiang Yang,[†] Xiaoyi Zhang,[§] Cheslan K. Simpson,[†,⊗] Lin X. Chen,*[,‡,○] and Michael D. Hopkins*[,†]

[†]Department of Chemistry, The University of Chicago, 929 East 57th Street, Chicago, Illinois 60637, United States

[‡]Chemical Sciences and Engineering Division and [§]X-ray Sciences Division, Argonne National Laboratory, 9700 South Cass Avenue, Argonne, Illinois 60439, United States

Supporting Information

ABSTRACT: The molecular structure of the tungsten−benzylidyne complex *trans*-W(≡CPh)(dppe)$_2$Cl (**1**; dppe = 1,2-bis(diphenylphosphino)ethane) in the singlet $(d_{xy})^2$ ground state and luminescent triplet $(d_{xy})^1(\pi^*(WCPh))^1$ excited state (**1***) has been studied using X-ray transient absorption spectroscopy, X-ray crystallography, and density functional theory (DFT) calculations. Molecular-orbital considerations suggest that the W−C and W−P bond lengths should increase in the excited state because of the reduction of the formal W−C bond order and decrease in W→P π-backbonding, respectively, between **1** and **1***. This latter conclusion is supported by comparisons among the W−P bond lengths obtained from the X-ray crystal structures of **1**, $(d_{xy})^1$-configured **1**$^+$, and $(d_{xy})^2$ [W(CPh)(dppe)$_2$(NCMe)]$^+$ (**2**$^+$). X-ray transient absorption spectroscopic measurements of the excited-state structure of **1*** reveal that the W−C bond length is the same (within experimental error) as that determined by X-ray crystallography for the ground state **1**, while the average W−P/W−Cl distance increases by 0.04 Å in the excited state. The small excited-state elongation of the W−C bond relative to the M−E distortions found for M(≡E)L$_n$ (E = O, N) compounds with analogous $(d_{xy})^1(\pi^*(ME))^1$ excited states is due to the π conjugation within the WCPh unit, which lessens the local W−C π-antibonding character of the π^*(WCPh) lowest unoccupied molecular orbital (LUMO). These conclusions are supported by DFT calculations on **1** and **1***. The similar core bond distances of **1**, **1**$^+$, and **1*** indicates that the inner-sphere reorganization energy associated with ground- and excited-state electron-transfer reactions is small.

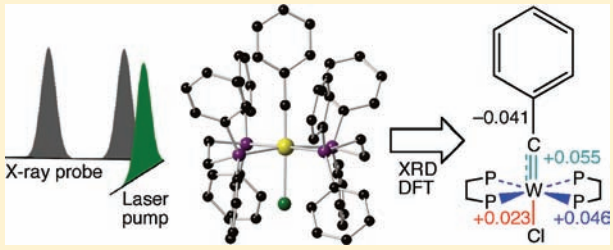

INTRODUCTION

The excited-state structures of luminescent metal−alkylidyne (carbyne) compounds[1] have not been the subject of detailed study. Knowledge of the structure of the luminescent excited state is important in fundamental contexts such as understanding the radiative and nonradiative decay of the state, the products and mechanisms of its photochemical reactions, and the reorganization energies associated with excited-state processes. These issues are pertinent for luminescent metal−alkylidyne complexes because they are interesting candidates for development as tunable photoredox chromophores. The structural and electronic diversity of luminescent metal−alkylidyne compounds is striking: this class includes complexes of the group 6, 7, and 8 transition metals, with formal d-electron counts of d^0, d^1, and d^2; structures that include tetrahedral, trigonal-bipyramidal, square-pyramidal, and octahedral geometries, supported by ancillary ligands that span the spectrochemical series; and a variety of luminescent excited states (d → π^*(M≡CR), π(M≡CR) → d, and metal-to-ancillary-ligand MLCT).[1−19] Further, the presence of the metal−carbon triple bond in these compounds means they can be used as building blocks for π-conjugated materials, the photophysical and redox functionality of which is substantially altered from those of their all-carbon analogues.[5,14,18,20−23] It has been suggested on the basis of photophysical and photochemical studies that some metal−alkylidyne compounds may possess a bent MCR linkage in the excited state,[3,4,18,24] and that the overall extent of distortion is likely to be small,[7] but direct excited-state structural probes have not been applied to these compounds.

We report an investigation of the ground-state and excited-state structures of the luminescent metal−alkylidyne compound *trans*-W(≡CPh)(dppe)$_2$Cl (**1**; dppe = 1,2-bis(diphenylphosphino)ethane; Scheme 1) using X-ray transient absorption spectroscopy,[25−30] X-ray crystallography, and density functional theory (DFT) calculations. This compound was selected for study because it is representative of the large class of d^2 metal−alkylidyne compounds that possess luminescent $^3[(d_{xy})^1(\pi^*(MCR))^1]$ excited states (**1***, Scheme 1).[1] These chromophores are electronically analogous to triply bonded d^2 metal−oxo and metal−nitrido complexes with luminescent $^3[(d_{xy})^1(\pi^*(MO))^1]$ and $^3[(d_{xy})^1(\pi^*(MN))^1]$ excited states, the structural distortions of which have been

Received: December 5, 2011
Published: February 28, 2012

   dx.doi.org/10.1021/ic202622s | *Inorg. Chem.* 2012, 51, 5660−5670

Scheme 1. Electron Configurations of 1, 1⁺, 1*, and 2⁺

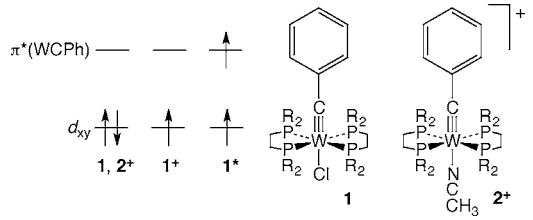

well studied and provide points of comparison for **1**.[31−36] The ground-state molecular structures of the one-electron oxidized congener $[W(CPh)(dppe)_2Cl]^+$ (**1**⁺) and of d^2 $[W(CPh)(dppe)_2(NCCH_3)]^+$ (**2**⁺) were determined to probe the structural consequences of d_{xy} electron configuration (**1**, $(d_{xy})^2$; **1**⁺, $(d_{xy})^1$) and of charge (**2**⁺), as illustrated in Scheme 1. We have found that the elongation of the WC bond for **1*** in the $^3[(d_{xy})^1(\pi^*(WCR))^1]$ state is substantially less than that of the ME bonds (E = O, N) of metal−oxo and metal−nitrido compounds in corresponding $(d_{xy})^1(\pi^*(ME))^1$ excited states, and than those of the tungsten−ancillary-ligand bonds. The magnitudes of these distortions reflect the orbital character of the luminescent state.

EXPERIMENTAL SECTION

General Procedures. All experiments were performed under a nitrogen atmosphere using standard Schlenk and glovebox techniques. HPLC-grade solvents, stored under nitrogen in stainless-steel cylinders, were purified by passing them under nitrogen pressure through an anaerobic, stainless-steel system consisting of either two 4.5 in. × 24 in. (1 gal) columns of activated A2 alumina (CH_3CN, Et_2O, CH_2Cl_2, and tetrahydrofuran (THF)) or one column of activated A2 alumina and one column of activated BASF R3-11 catalyst (toluene).[37] Benzene was dried over Na/K alloy, from which it was transferred under vacuum. Dichloromethane-d_2 was stirred over P_2O_5 for 48 h, from which it was transferred under vacuum and stored under nitrogen. The compound $W(CPh)(dppe)_2Cl$ (**1**) was prepared by the standard procedure;[38] crystals of $\mathbf{1}\cdot CH_2Cl_2$ suitable for single-crystal X-ray diffraction studies were grown from a concentrated solution of **1** in CH_2Cl_2 layered with Et_2O and cooled to −35 °C for 2 d. All other reagents were obtained from commercial sources and used as received.

^1H-, $^{13}C\{^1H\}$-, and $^{31}P\{^1H\}$-NMR spectra were recorded using Bruker AF-500 or DRX 400 MHz NMR spectrometers of samples in CD_2Cl_2 solution at room temperature. Chemical shifts were measured relative to solvent resonances (^1H and ^{13}C) or an external standard of 85% H_3PO_4 (^{31}P). Elemental analyses were performed by Midwest Microlabs (Indianapolis, IN) and Desert Analytics (Tucson, AZ). Electronic-absorption spectra were recorded using an Agilent Technologies 8453 UV−visible spectrophotometer of samples sealed in quartz cuvettes. Emission spectra were recorded on a PTI Quantmaster fluorimeter equipped with Peltier-cooled photomultiplier tube (R928) and InGaAs array detectors; emission intensities were corrected for instrument sensitivity.[39] Samples for emission measurements were prepared on a vacuum line, degassed with multiple freeze/pump/thaw cycles, and sealed under purified nitrogen. Emission quantum yields were determined relative to $[Ru(bpy)_3]Cl_2$ in N_2-saturated H_2O (ϕ_{em} = 0.063),[40] using absorbance-matched reference and analyte samples; a correction for the refractive index of the solvent was applied.[41] Electron paramagnetic resonance (EPR) spectra were measured with a Bruker Elexsys E500 CW EPR spectrometer (X band) using a SHQE cylindrical resonator, and processed with Bruker XEPR software (ver. 2.4b.10).

$[W(CPh)(dppe)_2(NCMe)][BPh_4]$ ([2][BPh$_4$]). To a stirred, room-temperature solution of **1** (0.50 g, 0.45 mmol) in THF (15 mL) was added MeCN (1 mL, excess) and $NaBPh_4$ (0.19 g, 0.54 mmol). The flask was sealed, and the reaction mixture heated to 70 °C for 12 h, during which the color changed from orange to brick red. (No reaction is observed between **1** and $NaBPh_4$ in THF in the absence of acetonitrile under otherwise identical reaction conditions.) After cooling the reaction mixture to room temperature, the solvent was removed in vacuo and the residue extracted with CH_2Cl_2 (ca. 20 mL). The resulting red solution was filtered through Celite and reduced to dryness under vacuum. The remaining solid was dissolved in acetonitrile (ca. 10 mL); this was layered with Et_2O (ca. 10 mL) and cooled to −35 °C. After 2 d, brick-red crystals of $[\mathbf{2}][BPh_4]\cdot NCMe\cdot OEt_2$ were isolated (0.60 g, 0.39 mmol, 86% yield). Interstitial diethyl ether and acetonitrile can be removed by heating the crystals to 60 °C under vacuum for 12 h. ^1H NMR (400.13 MHz, CD_2Cl_2): δ 7.42 (br m, 8 H, *o*-PPh_2), 7.32 (overlapping m, 12 H, *o*-BPh_4 and *p*-PPh_2), 7.27 (t, 4 H, *p*-PPh_2), 7.19 (t, 1 H, $^3J_{HH}$ = 7.4 Hz, *p*-WCPh), 7.11 (t, 8 H, *m*-BPh_4), 7.02 (m, 16 H, *m*-PPh_2), 6.89 (overlapping m, 6 H, *m*-WCPh and *p*-BPh_4), 6.75 (br m, 8 H, *o*-PPh_2), 6.42 (d, 2 H, $^3J_{HH}$ = 7.6 Hz, *o*-WCPh), 2.81 (br m, 4 H, PCH_2), 2.61 (br m, 4 H, PCH_2), 0.74 (s, 3 H, MeCN). $^{13}C\{^1H\}$ NMR (100.6 MHz, CD_2Cl_2): δ 270.9 (W≡C), 164.6 (m, *ipso*-BPh_4), 151.1 (*ipso*-

Table 1. Crystal Data and Data Collection and Refinement Parameters for $W(CPh)(dppe)_2Cl$ (1), $[W(CPh)(dppe)_2(NCCH_3)][BPh_4]$ ([2][BPh$_4$]), and $[W(CPh)(dppe)_2Cl][OTf]$ ([1][OTf])

parameter	$\mathbf{1}\cdot CH_2Cl_2$	$[\mathbf{2}][BPh_4]\cdot MeCN\cdot Et_2O$	$[\mathbf{1}][OTf]\cdot 2CH_2Cl_2$
formula	$C_{60}H_{55}Cl_3P_4W$	$C_{91}H_{89}BN_2OP_4W$	$C_{61}H_{55}Cl_3P_4F_3SO_3W$[a]
space group	$P2_1/c$	$P\bar{1}$	$P\bar{1}$
a, Å	11.1414(19)	13.266(3)	11.195(3)
b, Å	26.800(5)	16.373(3)	12.247(3)
c, Å	19.120(3)	18.470(4)	22.433(6)
α, deg	90	97.281(3)	102.834(5)
β, deg	117.687(8)	108.399(3)	90.439(5)
γ, deg	90	96.291(3)	97.102(5)
V, Å^3	5055.3(15)	3728.1(13)	2973.9(13)
Z	4	2	2
ρ_{calcd}, g cm^{-3}	1.564	1.377	1.475
μ, mm^{-1}	2.611	1.686	2.250
GOF on F^2	1.089	1.045	1.058
final *R* indices [$I > 2\sigma(I)$]	*R*1 = 0.0408	*R*1 = 0.0257	*R*1 = 0.0520
	*wR*2 = 0.1074	*wR*2 = 0.0631	*wR*2 = 0.0927
final *R* indices (all data)	*R*1 = 0.0434	*R*1 = 0.0271	*R*1 = 0.0657
	*wR*2 = 0.1090	*wR*2 = 0.0637	*wR*2 = 0.0971

[a]Formula based on refined structure, which excludes one CH_2Cl_2 molecule.

dx.doi.org/10.1021/ic202622s | Inorg. Chem. 2012, 51, 5660−5670

WCPh), 138.5 (m, *ipso*-PPh_2), 136.5 (BPh_4), 135.8 (m, *ipso*-PPh_2), 133.9 (*o*-PPh_2), 132.9 (*o*-PPh_2), 130.6 (*p*-PPh_2), 130.3 (*p*-PPh_2), 128.9 (*m*-PPh_2), 128.6 (*m*-PPh_2), 127.8 (WCPh), 126.2 (BPh_4), 122.3 (BPh_4), 32.26 (m, PCH_2), 2.87 (MeCN); two WCPh resonances and MeCN were not observed. $^{31}P\{^1H\}$ NMR (161.9 MHz, CD_2Cl_2): δ 53.0 (s, $^1J_{PW}$ = 281 Hz). IR (neat film): 2305 cm^{-1} (MeC≡N). UV−vis (CH_2Cl_2), λ_{max}/nm (ε_{max}/M^{-1} cm^{-1}): 260 (sh, 41100), 340 (16900), 470 (sh, 830), 545 (300), 850 (sh, 5); see Supporting Information, Figure S1. Anal. Calcd (found) for $C_{85}H_{76}BNP_4$: C 71.39 (71.56), H 5.36 (5.89), N 0.98 (0.81).

[W(CPh)(dppe)$_2$Cl][OTf] ([1][OTf]). Solutions of **1** (0.20 g, 0.181 mmol) in CH_2Cl_2 (25 mL) and AgOTf (0.045 g, 0.175 mmol) in CH_2Cl_2 (20 mL) were cooled to −35 °C, combined with stirring, and allowed to warm to room temperature. Upon mixing the color of the solution changed from orange to dark red-orange, and a dark precipitate of silver formed. After 90 min the reaction mixture was filtered though Celite, and the flask and filter contents washed with CH_2Cl_2 (3 × 20 mL). The filtrate was reduced to dryness under vacuum, leaving a red residue. The residue was washed with benzene (3 × 30 mL) to remove unreacted **1**; the final washing was colorless. The product [**1**][OTf] was recrystallized by slow diffusion of Et_2O vapor into a saturated CH_2Cl_2 solution of the compound at room temperature; this provided red crystals of [**1**][OTf]·$2CH_2Cl_2$ suitable for X-ray diffraction studies. Crystals washed with Et_2O and dried under vacuum at 60 °C overnight provided [**1**][OTf] as a red powder in 88% yield (0.213 g, 0.160 mmol). ^1H NMR (CD_2Cl_2, 500.13 MHz): δ 9.57 (v br), 8.31 (br), 8.23 (br), 7.80 (br), 7.70 (br); very weak, sharp resonances are also observed at δ 7.41 (m), 7.11 (t), 6.69 (t), 5.66 (d), and 3.03 (br) that are ascribed to the trace impurity [W(CPh)(H)(dppe)$_2$Cl][OTf]. $^{31}P\{^1H\}$ NMR (CD_2Cl_2): no signal observed. UV−vis (CH_2Cl_2), λ_{max}/nm (ε_{max}/M^{-1} cm^{-1}): 265 (sh, 20000), 320 (11700), 402 (sh, 1300), 510 (2700), 798 (35), 1050 (40); see Supporting Information, Figure S2. EPR (CH_2Cl_2, 306 K): $\langle g\rangle$ = 2.055, $\langle a(^{31}P)\rangle$ = 30.6 G; see Supporting Information, Figure S3. ESI-MS (*m*/*z*): 1103.9 [M^+]. Anal. Calcd (found) for $C_{60}H_{53}ClF_3O_3P_4SW$: C 57.45 (57.05); H 4.26 (4.54).

Single-Crystal X-ray Diffraction Studies. X-ray diffraction data were collected with a Bruker SMART APEX system using graphite-monochromated MoKα (λ = 0.71073 Å) radiation of crystals coated in Fluorolube oil and cooled to 100 K. A hemisphere (**1**·CH_2Cl_2, [**2**][BPh_4]·MeCN·Et_2O) or full sphere ([**1**][OTf]·$2CH_2Cl_2$) of data was acquired. Integration of intensities and refinement of cell parameters were obtained using SAINT (ver. 6.02) and absorption corrections were applied using SADABS (ver. 2.03). Structures were solved using SHELXTL (ver. 5.1).[42] Crystal data and data collection and refinement parameters are collected in Table 1.

For **1**·CH_2Cl_2, two phenyl rings on the dppe ligands (C(28)−C(33) and C(54)−C(59)) have elongated displacement ellipsoids consistent with positional disorder. For [**1**][OTf]·$2CH_2Cl_2$, the two interstitial CH_2Cl_2 sites were partially occupied and one of the two CH_2Cl_2 molecules was disordered. Following anisotropic refinement of all non-H atoms, the occupancy of the ordered CH_2Cl_2 molecule was refined and the disordered CH_2Cl_2 molecule was excluded from the structure. The structure was SQUEEZEd to account for the disordered molecule, which accounted for 60 electrons/cell. The occupancy of the other CH_2Cl_2 molecule was 0.77.

X-ray Absorption Spectroscopy (XAS). Samples of **1** in toluene (8×10^{-4} M) were prepared under nitrogen atmosphere in a glovebox and transferred to a flow cell via syringe. X-ray transient absorption (XTA) or laser-initiated time-resolved X-ray absorption spectroscopy (LITR-XAS) measurements[25,26,28−30] at the tungsten L_{III}-edge (10.204 keV) were conducted at a dual inline undulator insertion device beamline, 11ID-D, at the Advanced Photon Source in Argonne National Laboratory. A monochromator with Si 111 crystals provided an energy resolution of ∼1.2 eV at 10 keV. A laser pump pulse is used to synchronously trigger a photochemical reaction in an ensemble of molecules, followed by an X-ray probe pulse used to take the XAS spectrum of the sample as a result of the photoexcitation. This pump−probe cycle is repeated at 1 kHz. The X-ray probe pulses (∼10^6−10^7 photons/pulse at 10 keV) were extracted from a train of electron bunches circulating in the storage ring under a 24-bunch mode with 0.015% of the total flux at 1 kHz. Two plastic scintillator coupled photomultiplier tube (PMT) detectors were placed at a right angle from the incident X-ray beam on both sides of the liquid sample jet. Custom designed cylindrical soller slits with a zinc filter were placed in front of the detector to remove most of the elastically scattered photons and prevent detector saturation. The detectors were used in a current mode to allow multiple X-ray fluorescence photons from the sample originating from a single X-ray probe pulse to be collected. The two detector units were connected to a fast digitizing board (Agilent) enabling signals originating from all X-ray pulses between two laser pump pulses to be recorded. The third detector of the same kind without the soller slits/Zn filter was used for the intensity normalization, which was placed at a right angle from the X-ray beam to collect X-ray photons through elastic scattering from a carbon film placed in the upstream of the X-ray beam from the sample. The instrument response function was ∼5 ns fwhm. The delay time between the laser and the X-ray pulses was adjusted by a programmable delay line (PDL-100A-20NS, Colby Instruments) that adjusts the phase shift of the mode-lock driver for the seed laser relative to that of the RF signal of the storage ring with a precision of 500 fs without mechanical movement. The XTA spectra were collected with a total data acquisition time of approximately 20 h, or about 40 scans. The integrity of the sample was ascertained by monitoring the UV−visible and X-ray absorption spectra of the ground state. If changes were observed the sample was replaced.

The pump laser pulses for creating the excited state molecules were from the third harmonic output of a Nd:YLF regenerative amplifier laser (λ = 351 nm, 1 kHz, ∼0.4 mJ/pulse and 5 ps fwhm at the sample). To adjust the time delay between the pump and the probe pulses, a Si PIN diode was used to collect signals from the laser and the X-ray pulses simultaneously, and the time delays between them were adjusted accordingly. The accuracy of the delay time is ∼50 ps limited by the PIN diode response time. The delay time between the pump and the probe was set to nominally 50 ps (i.e., with the laser pulse leading). The laser and X-ray beams were overlapped on a continuously flowing stream of 0.8 mM **1** solution jet with 0.5 mm thickness.

Data Analysis of XANES and XAFS Spectra. For the XAFS data analysis, the crystal structure of **1** was used as the reference for the ground state (R_{W-C} = 1.83 Å, R_{W-P} = 2.49 Å, and R_{W-Cl} = 2.54 Å). XAFS data analysis package Athena-Artemis was used following standard procedures. The experimentally collected data after the Fourier transform were fit to eq 1:[43−46]

$$\chi(k) = \sum F_i(k)\, {S_0}^2(k) N_i/(kR_i^2)\cdot\exp(-2\sigma_i^2 k^2) \sin[2kR_i + \phi_i(k)] \quad (1)$$

where $F(k)$ is the magnitude of the backscattering; S_0 is the amplitude reduction factor; N is the coordination number; R is the average distance; σ^2 is the Debye−Waller factor; ϕ_i is the phase shift; k is the electron wavevector; and the subscript indicates ith atom. The reference amplitudes and phases for the scattering paths were calculated by the FEFF6.0 program (University of Washington, FEFF project) included in the data analysis software package.[47−53]

Since photoexcitation did not produce an excited state population of 100%, the X-ray absorption spectrum of a laser pumped sample is a mixture of the ground and the excited-state spectra, as described by eq 2:

$$\mu(E, t) = [1 - f(t)]\mu_{gs}(E) + f(t)\mu_{es}(E) \quad (2)$$

Equation 2 is based on two approximations: (1) the spectrum is taken at a time delay between the pump and the probe pulses well beyond the vibrational relaxation from the initial Franck−Condon state to the thermally equilibrated excited state; and (2) there is only one thermally equilibrated excited state at the delay time. This is the case when the time resolution is limited by the X-ray pulse duration from the synchrotron source (80−100 ps), and only one excited state is populated. Therefore, the total absorption $\mu(E,t)$ at photon energy E is

dx.doi.org/10.1021/ic202622s | Inorg. Chem. 2012, 51, 5660−5670

the function of the ground state absorption $\mu_{gs}(E)$ and the excited state absorption $\mu_{es}(E)$, and $f(t)$ is the fraction of excited state molecules at t, and the subscripts gs and es stand for the ground and excited states, respectively. Further simplification can be made if the time delay between the laser pump and the X-ray probe pulses is set to probe the first detectable excited state structure at its optimal concentration, normally at time "zero", which is within 100 ps of the pump laser pulse in our experiments. Equation 2 can be simplified as:

$$\mu(E) = [1 - f_{es}(0)]\mu_{gs}(E) + f_{es}(0)\mu_{es}(E) \quad (3)$$

In general, $\mu_{es}(E)$ and $f_{es}(0)$ are both unknown, which imposes two unknowns in eq 3. The excited-state fraction $f_{es}(0)$ of **1*** in solution at the time delay of the XTA experiment was measured to be approximately 45%, as determined by optical transient-absorption measurements using the same laser source and the same sample concentration in toluene solution; this value is in agreement with that calculated from the Beer–Lambert law. This allowed $\mu_{es}(E)$ to be extracted and analyzed. Coordination numbers and energy shifts in the fits for both the ground state and the excited state spectra were kept the same.

Electronic Structure Calculations. Calculations on **1** and **1*** were performed using DFT, as implemented in Gaussian09.[54] Calculations employed the B3P86 functional,[55,56] which according to recent benchmarks ranks among the best functionals for predicting the molecular structures of third-row transitional metal complexes.[57,58] Geometries were optimized without symmetry constraints. No imaginary frequencies were obtained in subsequent vibrational calculations, confirming that the optimized structures (Supporting Information, Tables S1 and S2) reside at potential-surface minima. The overall basis set quality is approximately double-ζ plus polarization (DZP). The LANL2DZ effective-core potential (ECP) basis set,[59] augmented with an f-type polarization function,[60] was used for W. Dunning's full double-ζ plus polarization basis sets (DZP) were used for C, P, and Cl; for H, a double-ζ (DZ) basis set was used.[61,62] For comparison, a calculation of the ground-state structure of **1** was also conducted with triple-ζ-plus-polarization quality (TZP) basis sets: the Stuttgart/Dresden (SDD) ECP basis set,[63] supplemented by two f and one g polarization functions,[64] was used for W, and cc-pVTZ basis sets[65] were used for all other atoms. Both the DZP- and TZP-quality basis-set calculations gave molecular structures that are in satisfactory agreement with the crystal structure of **1**, so the former basis sets were used for the remaining calculations because of their substantially reduced computation-time demands. Time-dependent DFT (TD-DFT) calculations were performed on **1** at the optimized ground-state geometry. The calculations were carried out with the B3P86 functional and the DZP level basis sets described above, to which were added one set of diffuse functions for hydrogen and carbon and two sets of diffuse functions for P and Cl.[61,62] Atomic parentages of orbitals, based on Mulliken population analysis, were calculated with AOMix,[66] and those based on the molecular orbital analysis in the natural atomic orbital basis were calculated with the NBO program.[67] Orbital contours were rendered with the Arguslab program.[68]

RESULTS AND DISCUSSION

Electronic Structure and Spectra of W(CPh)(dppe)$_2$Cl (1). The assignment and molecular structure of the luminescent excited state of W(CPh)(dppe)$_2$Cl can be anticipated by consideration of the frontier molecular orbitals of the compound. The orbitals for an idealized C_{2v} symmetry d^2 M(CPh)L$_5$ compound, as considered from the standpoint of L$_5$M≡C and C$_6$H$_5$ fragments, are shown in Figure 1.[1] The highest occupied molecular orbital (HOMO) and lowest unoccupied molecular orbital (LUMO) are of metal d-orbital (t_{2g}) parentage. The HOMO ($2a_2$) is the metal-centered d_{xy} orbital, which is nonbonding (δ symmetry) with respect to the MC axis and π symmetry with respect to the equatorial ligands. The LUMO ($3b_1$), denoted π^*(MCPh), is the in-phase (π

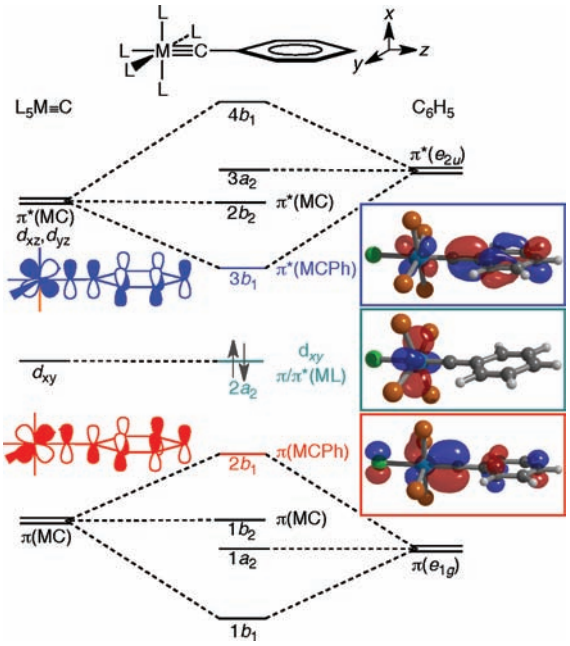

Figure 1. Qualitative molecular-orbital diagram for d^2 M(CPh)L$_5$, and calculated (DFT) orbital contours of the π^*(WCPh), d_{xy}, and π(WCPh) levels of W(CPh)(dppe)$_2$Cl (**1**). For clarity, the phenyl groups of the dppe ligands are not shown in the calculated contours.

bonding) combination between the out-of-plane π^*(M≡C) orbital (d_{xz} parentage) and a π^*(C$_6$H$_5$) orbital. The HOMO−1 ($2b_1$), denoted π(MCPh), is the corresponding out-of-phase (π^*) combination of π(M≡C) and π(C$_6$H$_5$). DFT calculations on **1** show that the nodal character and WCPh atomic parentage of the LUMO, HOMO, and HOMO−1 conform to this scheme, as indicated by the correspondence between the qualitative and calculated orbital surfaces shown in Figure 1. The calculated atomic parentage of the orbitals, set out in Table 2, reveals that the d_{xy} HOMO and π^*(WCPh) LUMO contain

Table 2. Calculated (DFT) Energies and Atomic Parentage of Selected Frontier Orbitals of W(CPh)(dppe)$_2$Cl (1)

			atomic parentage, %[a]			
orbital	no./ symmetry	energy (eV)	W	CPh	dppe	Cl
π^*(WCPh) (LUMO)	250a	−1.55	18.1	50.8	29.7	1.5
d_{xy} (HOMO)	249a	−4.89	74.0	0.0	25.9	0.0
π(WCPh) (HOMO−1)	248a	−5.56	30.1	47.8	9.7	12.4

[a]Based on Mulliken population analysis; contributions calculated via the NBO program are similar (Supporting Information, Table S3).

significant contributions from the dppe ligands; in the case of the HOMO, this interaction can be described as W → dppe π-backbonding in nature.

The lowest-energy electronic excited state expected for d^2 M(CPh)L$_5$ compounds is produced by the $d_{xy} \rightarrow \pi^*$(MCPh) HOMO → LUMO transition ($2a_2 \rightarrow 3b_1$ in Figure 1). The electronic-absorption spectrum of **1**, shown in Figure 2, exhibits a shoulder assigned to the spin- and dipole-allowed $^1[d_{xy} \rightarrow \pi^*(\text{WCPh})]$ transition as the lowest-energy feature (λ_{max} = 525 nm, ε = 310 M^{-1} cm^{-1}). The $^1[\pi(\text{WCPh}) \rightarrow \pi^*(\text{WCPh})]$ band ($2b_1 \rightarrow 3b_1$ in Figure 1) is observed at higher energy (λ_{max} =

dx.doi.org/10.1021/ic202622s | Inorg. Chem. 2012, 51, 5660–5670

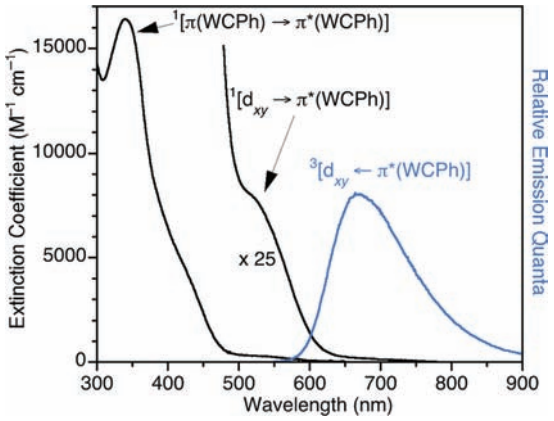

Figure 2. Electronic-absorption and -emission spectra of W(CPh)(dppe)$_2$Cl (**1**) in toluene solution at room temperature.

340 nm, ε = 16400 M^{-1} cm^{-1}). The positions and intensities of these bands are similar to those observed for the corresponding bands of related d^2 metal−benzylidyne compounds.[1] The assignment of the 525-nm band as $^1[d_{xy} \rightarrow \pi^*(WCPh)]$ is supported by a TD-DFT calculation, which places the spin-allowed electronic transition of principal $d_{xy} \rightarrow \pi^*(WCPh)$ parentage at 511 nm (94% 249a → 250a).[69]

Excitation into the $^1[d_{xy} \rightarrow \pi^*(WCPh)]$ (and higher energy) absorption bands of **1** in toluene solution at room temperature produces luminescence centered at 668 nm (Figure 2). The high-energy edge of the emission band overlaps with the red tail of the $^1[d_{xy} \rightarrow \pi^*(WCPh)]$ absorption band, suggesting it is also associated with a $(d_{xy})^1(\pi^*(WCPh))^1$ state; the long emission lifetime (τ = 303 ns in toluene solution at room temperature; ϕ = 0.017) indicates the excited state is of spin-triplet parentage. On the basis of these observations, the electron configuration of the emissive state is assigned as $^3[(d_{xy})^1(\pi^*(WCPh))^1]$ (**1***). The electronic-absorption spectrum does not exhibit a distinct feature attributable to the $^3[d_{xy} \rightarrow \pi^*(WCPh)]$ transition, but it presumably lies within the low-energy tail of the $^1[d_{xy} \rightarrow \pi^*(WCPh)]$ absorption band. On the basis of the fact that this absorption tail extends to λ > 650 nm (Figure 2), the 0−0 energy of the $^3[(d_{xy})^1(\pi^*(WCPh))^1]$ state is inferred to lie below 15500 cm^{-1}. Consistent with these assignments, the lowest-energy triplet state calculated by DFT is of configuration $^3[(d_{xy})^1(\pi^*(WCPh))^1]$ and lies 14759 cm^{-1} above the ground state (including zero-point energy correction).

The molecular structure of **1*** in the luminescent $^3[(d_{xy})^1(\pi^*(WCPh))^1]$ state is expected to be distorted relative to the $(d_{xy})^2$ ground state of **1** in ways that reflect their different $(d_{xy})^m(\pi^*(WCPh))^n$ configurations. On the basis of the orbital characteristics described above, the principal effect of depopulating the d_{xy} orbital in the excited state is to reduce W → dppe π backbonding; this should lengthen the W−P bonds of **1*** relative to those of **1**. Population of the π^*(WCPh) orbital in the excited state will reduce the formal W−C bond order from 3.0 to 2.5 and increase the WC−C_{ipso}(Ph) bond order from 1.0 to 1.5; this should result in lengthening of the W−CPh bond and shortening of the WC−C_{ipso}(Ph) bond in the excited state relative to the ground state. On the basis of molecular-orbital considerations alone the W−Cl bond is not expected to be strongly affected by population of the $(d_{xy})^1(\pi^*(WCPh))^1$ excited state, because it is orthogonal to the d_{xy} orbital and contributes little to the π^*(WCPh) orbital (0% and 1.5% contributions, respectively; Table 2).

Single-Crystal X-ray Diffraction Studies of W(CPh)(dppe)$_2$Cl (1), [W(CPh)(dppe)$_2$Cl]$^+$ (1$^+$), and [W(CPh)(dppe)$_2$(NCMe)]$^+$ (2$^+$). The molecular structures of the compounds **1**, [**1**][OTf], and [**2**][BPh_4] were determined by X-ray crystallography to provide points of reference for interpreting the excited-state structure of **1***. The electron configurations of the compounds are illustrated in Scheme 1. Comparison of the structure of **1**$^+$ to that of **1** allows the effects of $(d_{xy})^m$ configuration to be probed (**1**, $(d_{xy})^2$; **1**$^+$, $(d_{xy})^1$); this is relevant to the structure of **1*** because the $^3[(d_{xy})^1(\pi^*(WCPh))^1]$ excited state also possesses a singly occupied d_{xy} orbital. The structure of the $(d_{xy})^2$ ion **2**$^+$ provides a control for any structural manifestions of overall charge that might complicate the comparison between **1**$^+$ and **1**.

The structures of **1**, **1**$^+$, and **2**$^+$ are shown in Figures 3−5, respectively, and important bond distances and bond angles are set out in Table 3. All compounds exhibit a pseudo-octahedral geometry about the tungsten center with the benzylidyne ligand oriented *cis* to the phosphorus atoms of the dppe ligands and trans to the chloride or acetonitrile ligand, as found for other d^2- and d^1-configured compounds of the type W(CR)L_4X (L = phosphine).[21,70−79] The plane of the benzylidyne phenyl group bisects the ethylene backbones of the dppe ligands. Although the solution-phase NMR data for **1** and **2**$^+$ are consistent with high-symmetry structures, the geometries of the WCP_4X units in the solid state are significantly distorted from idealized C_{2v} symmetry; for all compounds, sizable ranges are spanned by the chemically equivalent W−P bond distances (Δd = 0.03−0.05 Å) and C≡W−P angles ($\Delta\theta$ = 4.5−10.2°). The structures of analogous compounds of the form W(CR)(dmpe)$_2$X (dmpe = 1,2-bis(dimethylphosphino)ethane)[72,74−79] are much less irregular than those for **1**, **1**$^+$, and **2**$^+$, suggesting that the distortions

Table 3. Selected Bond Distances (Å) and Bond Angles (deg) for 1, [2][BPh$_4$], and [1][OTf][a]

nuclei	**1**	[**2**][BPh_4]	[**1**][OTf]
W≡C(1)	1.833(5)	1.8281(19)	1.826(6)
C(1)−C(2)	1.441(8)	1.450(3)	1.444(8)
W−P(1)	2.4819(14)	2.4743(6)	2.5888(19)
W−P(2)	2.4898(14)	2.4607(7)	2.5784(18)
W−P(3)	2.5056(14)	2.5019(7)	2.5354(19)
W−P(4)	2.4749(14)	2.5103(7)	2.5712(18)
W−P_{avg}	2.4881[14]	2.4868[7]	2.5685[19]
W−X (X = Cl, N)	2.5373(14)	2.2701(17)	2.5153(17)
C(1)−W−X (X = Cl, N)	177.05(17)	178.59(7)	177.7(2)
C(2)−C(1)−W	178.3(4)	177.03(15)	178.2(5)
P(1)−W−P(2)	79.62(5)	79.345(18)	79.92(6)
P(2)−W−P(3)	99.74(5)	98.636(18)	96.76(6)
P(3)−W−P(4)	80.00(5)	79.300(17)	79.15(6)
P(4)−W−P(1)	100.33(5)	102.240(18)	103.89(6)
P(1)−W−P(3)	177.98(5)	169.227(17)	176.44(6)
P(2)−W−P(4)	170.98(5)	176.864(15)	169.35(5)
C(1)−W−P(1)	90.04(16)	90.66(6)	93.5(2)
C(1)−W−P(2)	94.45(16)	89.72(6)	97.55(19)
C(1)−W−P(3)	91.91(16)	99.94(6)	88.2(2)
C(1)−W−P(4)	94.57(16)	92.96(6)	92.18(19)
C(1)−W−P_{avg}	92.74[16]	93.32[6]	92.9[2]

[a]Values in square brackets are the mean of the standard deviations.

dx.doi.org/10.1021/ic202622s | *Inorg. Chem.* 2012, 51, 5660−5670

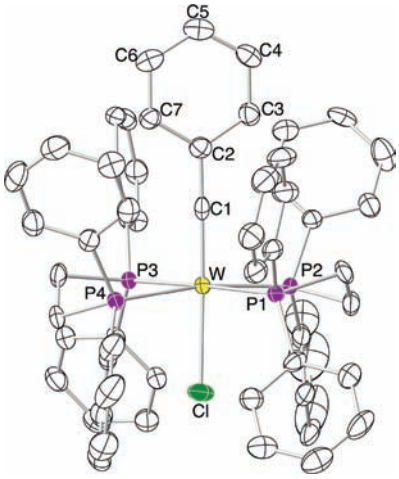

Figure 3. Thermal-ellipsoid representation of the structure of W(CPh)(dppe)$_2$Cl (**1**) from the crystal structure of **1**·CH_2Cl_2 (50% probability ellipsoids). Hydrogen atoms and interstitial dichloromethane are omitted for clarity.

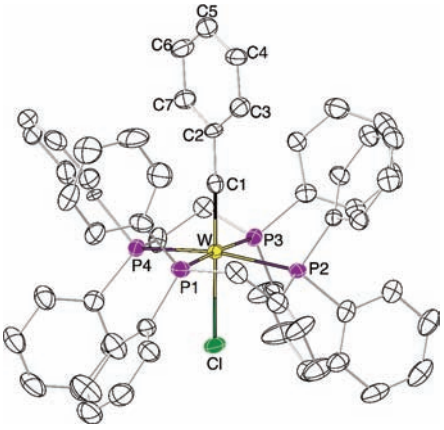

Figure 4. Thermal-ellipsoid representation of the structure of the [W(CPh)(dppe)$_2$Cl]$^+$ (**1**$^+$) ion of [**1**][OTf]·$2CH_2Cl_2$ (50% probability ellipsoids). Hydrogen atoms are omitted for clarity.

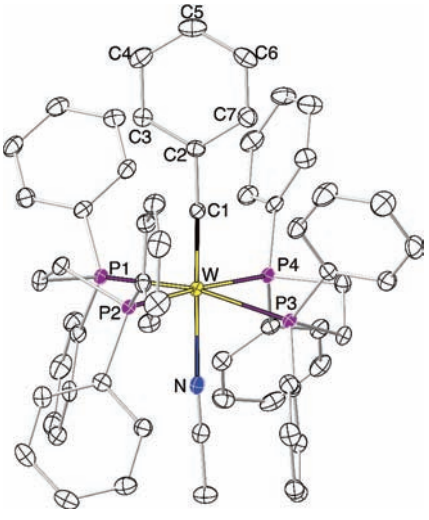

Figure 5. Thermal-ellipsoid representation of the structure of the [W(CPh)(dppe)$_2$(NCCH$_3$)]$^+$ (**2**$^+$) ion of [**2**][BPh_4]·MeCN·Et_2O (50% probability ellipsoids). Hydrogen atoms are omitted for clarity.

observed for the latter are the result of avoided contacts among their sterically demanding dppe ligands.[80]

Comparisons among the metrical data for **1**, **1**$^+$, and **2**$^+$ are confined to the W≡C, W−P, and W−Cl bond distances, which are those probed for the excited state **1*** by XTA measurements; the other bond distances and angles are unremarkable. The W≡C bond distances of the three compounds lie within a 0.01-Å range and are statistically indistinguishable from one another (**1**, 1.833(5) Å; **1**$^+$, 1.826(6) Å; **2**$^+$, 1.8281(2) Å), consistent with the fact that all possess a formal W≡C bond order of 3.0. In contrast, the W−P and W−Cl bond lengths of **1** and **1**$^+$ show a dependence on $(d_{xy})^m$ configuration: the average W−P bond distance for $(d_{xy})^1$ **1**$^+$ is 0.08 Å longer than for $(d_{xy})^2$ **1**, and the W−Cl bond distance of **1**$^+$ is shorter than that of **1** by 0.022 Å. These observations parallel the trends in W−P and W−X distances reported for other analogous d^2/d^1 pairs of tungsten−alkylidyne compounds ([W(CPh)(dmpe)$_2$Br]$^{0/+}$, Δd(W−P) = +0.053 Å, Δd(W−Br) = −0.042 Å);[72] [W(CH)(dmpe)$_2$Cl]$^{0/+}$, Δd(W−P) = +0.06 Å, Δd(W−Cl) = −0.05 Å).[74] The increase in W−P distance between **1** and **1**$^+$ is not attributable to the increased charge on **1**$^+$, since the $(d_{xy})^2$ complexes **1** and **2**$^+$ exhibit nearly identical average W−P bond lengths (**1**, 2.4881 (1) Å; **2**$^+$, 2.4868 (7) Å). Instead, the increase in W−P bond length for **1**$^+$ is likely due to the reduction in W → dppe π backbonding with the $(d_{xy})^1$ configuration, as anticipated from the molecular-orbital arguments above.[81] The 0.022 Å contraction of the W−Cl bond in **1**$^+$ relative to **1** does not have a simple molecular orbital explanation; the d_{xy} orbital is nonbonding with respect to the W−Cl bond, and so the formal bond order (1.0) is identical for both **1** and **1**$^+$. Instead, the W−Cl contraction probably reflects electrostatic and/or ionic-radius factors ($r(W^{IV})-r(W^V)$ = 0.04 Å).[82]

DFT Calculations of the Ground-State and Triplet Excited-State Structures of W(CPh)(dppe)$_2$Cl. The molecular structures of W(CPh)(dppe)$_2$Cl in its electronic ground state (**1**) and lowest-energy triplet excited state (**1***) were calculated using DFT to provide a framework for interpreting the X-ray transient absorption spectroscopic experiments. The calculated ground-state bond distances and angles for **1** are set out in Table 4. As is observed in the crystal structure, the calculated structure exhibits a trans pseudo-octahedral geometry with irregular W−P distances and C≡W−P angles and with the plane of the benzylidyne phenyl group bisecting the ethylene backbones of the dppe ligands. The calculated metrical data are in satisfactory agreement with those provided by the crystal structure of the complex; calculated bond distances within the W(CPh)P_4Cl core lie within 0.03 Å of the experimental values (Δ(**1**$_{calc}$ − **1**$_{exp}$), Table 4), and most bond angles differ by <2°.[83]

The calculated molecular structure of W(CPh)(dppe)$_2$Cl in the $^3[(d_{xy})^1(\pi^*(WCPh))^1]$ excited state (**1***) exhibits changes in bond lengths and bond angles relative to those of the $(d_{xy})^2$ ground state (**1**) that are consistent with expectations given the different electron configurations of the states (vide supra). The excited-state metrical data and their differences with respect to the ground state (Δ(**1***$_{calc}$ − **1**$_{calc}$)) are set out in Table 4. Within the WCPh unit, the largest excited-state distortion is a lengthening of the WC bond by 0.055 Å; this results from the reduction in formal W−C bond order in the excited state from 3.0 to 2.5. This is accompanied by a contraction of the WC−C_{ipso} bond (C_1−C_2) by 0.041 Å, which follows from the fact that the formal C_1−C_2 bond order increases from 1.0 for **1** to

dx.doi.org/10.1021/ic202622s | Inorg. Chem. 2012, 51, 5660−5670

Table 4. Selected Bond Distances (Å) and Angles (deg) for W(CPh)(dppe)$_2$Cl in the Ground State (1) and $^3[(d_{xy})^1(\pi^*(WCPh))^1]$ Excited State (1*) Calculated by DFT

nuclei	$\mathbf{1}_{calc}$	$\Delta(\mathbf{1}_{calc} - \mathbf{1}_{exp})^a$	$\mathbf{1}^*_{calc}$	$\Delta(\mathbf{1}^*_{calc} - \mathbf{1}_{calc})$
W≡C(1)	1.8156	−0.017(5)	1.8710	0.0554
C(1)−C(2)	1.4452	0.004(8)	1.4039	−0.0413
W≡C(1) + C(1)−C(2)	3.2608	−0.013[7]	3.2749	0.0141
W−P$_{min}$	2.4743	−0.0006(14)	2.5009	0.0266
W−P$_{max}$	2.5294	0.0238(14)	2.5791	0.0497
W−P$_{avg}$	2.4999	0.0118[14]	2.5454	0.0455
W−Cl	2.5661	0.0288(14)	2.5894	0.0233
C(2)−C(3)	1.4141	0.008(8)	1.4411	0.0270
C(3)−C(4)	1.3938	0.008(8)	1.3865	−0.0073
C(4)−C(5)	1.3999	0.026(9)	1.4087	0.0088
C(5)−C(6)	1.3993	0.021(9)	1.4083	0.0090
C(6)−C(7)	1.3945	0.016(8)	1.3872	−0.0073
C(7)−C(2)	1.4148	−0.003(8)	1.4409	0.0261
δr^b	0.0129	*c*	0.0379	0.0250
C(1)−W−Cl	178.68	1.63(17)	173.01	−5.67
C(2)−C(1)−W	178.29	0.0(4)	176.84	−1.45
cis P−W−P$_{min,avg}$	80.03	0.22(5)	81.03	1.10
cis P−W−P$_{max,avg}$	99.81	−0.23(5)	99.42	−0.39
C(1)−W−P$_{min}$	87.55	−4.36(16)	86.82	−0.73
C(1)−W−P$_{max}$	100.24	5.67(16)	102.28	2.04
C(1)−W−P$_{avg}$	93.40	0.66[16]	92.94	−0.46

[a]Experimental ground-state data for **1** are from the X-ray crystal structure (Table 3); values in parentheses are the crystallographic esd's, and those in square brackets their means. [b]$\delta r = 1/4[r(C(2)-C(3)) + r(C(4)-C(5)) + r(C(5)-C(6)) + r(C(7)-C(2)) - 2r(C(3)-C(4)) - 2r(C(6)-C(7))]$. [c]Within the benzylidyne phenyl group the C−C bonds involving the *ipso* carbon atom display the slight lengthening provided by the calculation, but it is of borderline statistical significance.

Table 5. Ground-State and Excited-State Internuclear Distances for 1 Determined by X-ray Crystallography and XAS[a]

	1					**1***	
nuclei[b]	$R_{crystal}$ (Å)	R_{XAS}[c] (Å)	σ^2 (Å^2)	R_{XAS}[d] (Å)	σ^2 (Å^2)	R_{XAS}[d] (Å)	σ^2 (Å^2)
W≡C(1)	1.833(5)	1.84(7)	0.0001	1.80	0.0007	1.79	0.0001
W−P	2.4881[14]	2.50(7)	0.0037				
W−Cl	2.5373(14)	2.49(7)	0.0001				
W−P/Cl				2.51	0.005	2.55	0.004
W···C(2)	3.274[7]	3.30(1)	0.001	3.30	0.001	3.32	0.0001

[a]XAS data are for samples in toluene solution; σ^2 is the Debye−Waller factor. [b]Values of *N* in eq 1 for scattering paths are as follows: W≡C, 1; W−P, 4; W−Cl, 1; W−P/Cl, 5, W···C(2), 2. [c]k = 3.4−13.0 Å^{-1}. [d]k = 3.5−10.0 Å^{-1}.

1.5 for **1***. As a result of these offsetting distortions, the distance between the W and C_{ipso} atoms is only slightly longer (by 0.014 Å) in the excited state than in the ground state. The WCC unit remains linear in **1***. The phenyl ring is predicted to undergo a quinoid-like distortion in the excited state (δr = 0.038 Å, Table 4), consistent with the partial multiple bond character in the C_1-C_2 linkage. The magnitude of the calculated C−C bond-length changes within the C−C_6H_5 unit are reasonable by comparison to those determined for the S_2 $\pi \rightarrow \pi^*$ excited state of phenylacetylene, which is the excited state analogous to the $2b_1 \rightarrow 3b_1$ $\pi \rightarrow \pi^*$ state for M(CPh)L_5 compounds (Figure 1). Specifically, in the S_2 state of phenylacetylene the formal HCC−C_{ipso} bond order increases from 1.0 to 2.0, which is twice the increase between **1** (1.0) and **1*** (1.5); the corresponding quinoid distortions for phenylacetylene (Δd(HCC−C_{ipso}) = −0.071 Å; δr = 0.072 Å) are, accordingly, roughly twice as large as those for **1*** ((Δd(WC−C_{ipso}) = −0.043 Å δr = 0.038 Å).[84] The calculated structure of **1*** also exhibits lengthened W−P and W−Cl bonds relative to the ground state. The W−P bond elongation (0.046 Å) is consistent with the reduction in W → dppe π backbonding upon depopulation of the d_{xy} orbital in the $(d_{xy})^1(\pi^*(WCPh))^1$ state. The W−Cl bond is predicted to be 0.023 Å longer in the excited state than the ground state. This distortion does not have a simple molecular-orbital explanation. The CPh ligand exerts a strong trans influence,[85] as manifested by the long W−Cl bond in the ground state of **1**; if the trans influence is decreased in the excited state because of the lengthening of the W−C bond, an excited state W−Cl bond contraction might have been anticipated.

Ground-State and Excited-State X-ray Absorption Spectroscopic (XAS) Studies of W(CPh)(dppe)$_2$Cl (1). Steady-state XAS measurements on **1** were conducted in solution to determine whether the structure of the compound is the same as that provided by its X-ray crystal structure, and to provide a baseline for its excited-state spectra (vide infra). The entire steady-state XAS spectrum spans an energy range from −100 to 800 eV relative to the W L_{III}-edge at 10.204 keV. The experimental XAS spectrum and the Fourier-transformed extended X-ray absorption fine structure (XAFS) region along with the theoretical fits are presented in Supporting Information, Figures S4 and S5. Atomic coordinates derived

dx.doi.org/10.1021/ic202622s | *Inorg. Chem.* 2012, 51, 5660−5670

from the crystal structure were used as the starting point for the theoretical fit. The data analyses for the steady-state spectrum in the range of k = 3.4−13.0 Å^{-1} provide the structural data set out in Table 5. The internuclear distances of **1** in solution are identical to those obtained from the X-ray crystal structure, within experimental error.

X-ray transient-absorption (XTA)[25] spectra of **1** in solution were obtained in a pump−probe experiment using pump excitation of 351 nm, which is within the $^1(\pi \rightarrow \pi^*)$ absorption band (λ_{max} = 340 nm, Figure 2). The experimental ground-state and 45% excited-state XAFS spectra of **1** and **1*** in toluene are shown in Figure 6. Because of experimental limitations on data

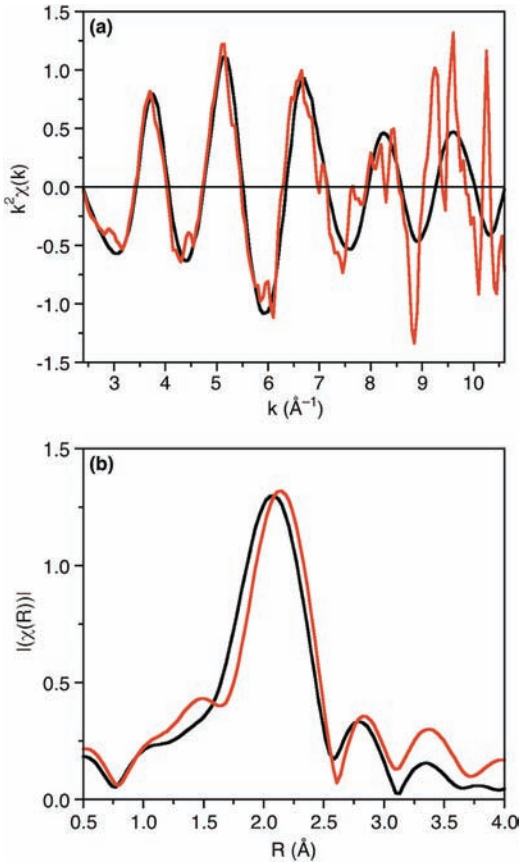

Figure 6. Experimental XAFS spectra of **1** (toluene solution): (a) in k; (b) after Fourier transform (nonphase shift corrected). Ground-state spectrum (black); 45% excited-state spectrum (red).

acquisition associated with the repetition rate of the laser pump pulses, the XTA spectrum has a lower signal-to-noise ratio than that of the steady-state XAS spectrum and the k range suitable for analysis (3.5−10.0 Å^{-1}) is narrower than that available in the steady-state XAS spectra described above (3.4−13.0 Å^{-1}).

Comparison of the ground-state and excited-state XAFS spectra (Figure 6a) reveals a higher-frequency oscillation in the latter, which corresponds to a shift to longer distances in the Fourier transform spectrum (Figure 6b). This observation suggests that there is an overall increase in the tungsten−ligand bond lengths in the excited state. A more quantitative assessment of the excited-state structural changes is provided by the fits in radial distribution functions after Fourier transform, which are shown in Figure 7; additional details regarding these fits are provided in Supporting Information. The structural parameters were extracted mainly for the nearest

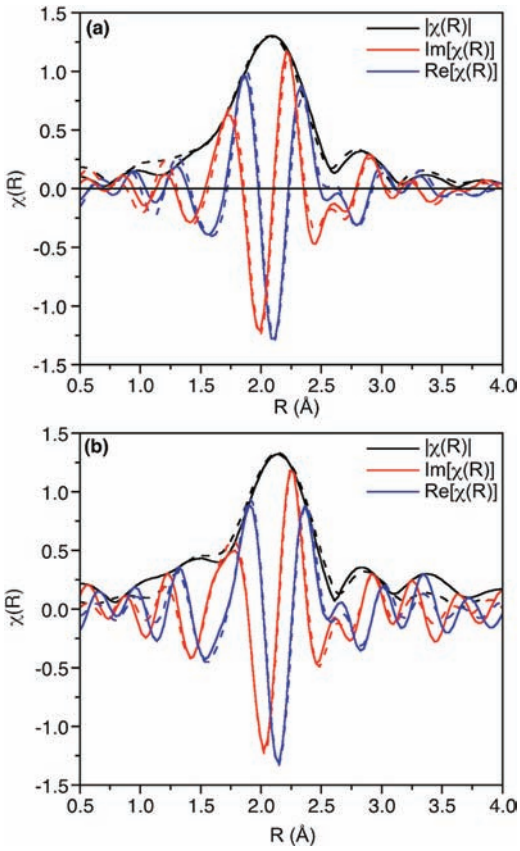

Figure 7. Fits (dotted lines) of Fourier transformed XAFS spectra (solid lines) of **1**, nonphase shift corrected: (a) ground state; (b) excited state.

neighbor distances because of the limited signal-to-noise ratio of the data, and only one distant C that is collinear with the W atom was included because of its enhanced intensity from a forward focusing effect. Further, it was difficult to accurately distinguish between the W−P and W−Cl scattering paths because of similarities in their bond lengths and the atomic numbers of backscattering atoms P (Z = 15) and Cl (Z = 17), as well as the narrow usable range in k space. Consequently, a single path representing the average distance of the four W−P paths and one W−Cl path was used for the fits. The results of these analyses are set out in Table 5. The ground-state internuclear distances derived from these data (k = 3.5−10.0 Å^{-1}) are similar to those derived from the steady-state spectra presented above (k = 3.4−13.0 Å^{-1}), as expected. The W−C(1) distance is difficult to accurately obtain because of the interference from multiple scattering paths; the best fits of the ground-state and excited-state spectra indicate that the W−C distance is the same, within error, in these states, while the two-bond W···C(2) distance appears to be slightly longer in the excited state (although this is at the edge of statistical significance). Fitting the large feature in the FT spectrum around 2 Å, which is dominated by the W−P and W−Cl scattering paths, indicates that the average W−P/W−Cl distance is elongated in the excited state by about 0.04 Å.

Analysis and Conclusions. The molecular and electronic structures, electronic spectra, and photophysical properties of W(CPh)(dppe)$_2$Cl are typical of those of the broader class of luminescent d^2 metal−alkylidyne complexes. Thus, it is reasonable to conclude that the excited-state structural distortions of this compound are representative of those of

dx.doi.org/10.1021/ic202622s | Inorg. Chem. 2012, 51, 5660−5670

related metal−alkylidyne luminophores. The differences between the structures of W(CPh)(dppe)$_2$Cl in the ground state (**1**) and luminescent excited state (**1***) are relatively small. Shown in Figure 8 are the bond-length changes for **1**$^+$ ((d$_{xy}$)^1

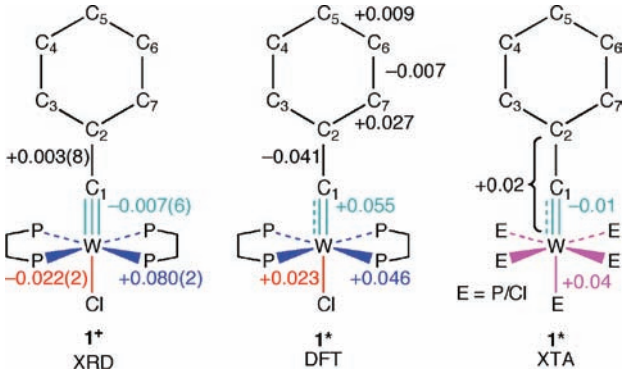

Figure 8. Bond-length changes (Å) for **1**$^+$ and **1*** relative to **1**.

configuration, Scheme 1) and **1*** ((d$_{xy}$)^1(π*(WCPh))^1) relative to **1** ((d$_{xy}$)^2), as determined by X-ray crystallography (Table 3), XAS (Table 5), and DFT calculations (Table 4). Considering first the W−Cl and W−P bonds, it is observed from the XAS data there is an overall (though not individually resolvable) lengthening of the bonds by 0.04 Å in the excited state relative to the ground state. This lengthening is very similar to the weighted average distortion of the W−P and W−Cl bond lengths predicted for **1*** by the DFT calculation (0.041 Å). On the basis of the molecular-orbital arguments outlined above, it is likely that the dominant contribution to the bond-length distortion measured by XAS is from the W−P bonds. Specifically, promotion of an electron from the d$_{xy}$ orbital to the π*(WCPh) orbital in the excited state is not expected to significantly affect the W−Cl bond, because Cl is a minor contributor to these orbitals (Table 2), whereas depopulation of the d$_{xy}$ orbital in the excited state weakens W → P π backbonding. The structural importance of this interaction is clearly manifested by the 0.08 Å elongation of the W−P bond in **1**$^+$ relative to **1** determined by X-ray crystallography. The DFT calculation for **1*** also predicts that the elongation of the W−P bonds in the excited state (by 0.046 Å) exceeds that of the W−Cl bond (0.023 Å).

The excited-state distortion of the W−C bond is near the detection limit of the X-ray transient absorption experiment. The DFT calculations on **1** and **1*** predict the W−C bond is 0.055 Å longer in the excited state than in the ground state; this is accompanied by a 0.041 Å contraction of the WC−C(2) bond and a small quinoid distortion of the benzylidyne phenyl group (Figure 8). These distortions reflect the decrease in the WC bond order from 3.0 to 2.5 and increase in the WC−C(2) bond order from 1.0 to 1.5 in the excited state (Figure 1). The XAS results indicate that the WC and two-bond W···C(2) distances are unchanged within experimental error, from which it may be concluded that the observed excited-state distortions within the WCC unit are no larger than those predicted from the DFT calculations. The observation that the W···C(2) distance for **1*** is similar to that of the ground state is inconsistent with substantial bending of the WCC linkage in the excited state, since such bending would shorten this distance. The DFT calculation on **1*** also predicts that the WCC unit remains linear in the excited state.

Context for the excited-state W−C bond-length distortion is provided by the excited-state M−E bond distances of the related triply bonded d^2 compounds Re(≡N)(PR$_3$)$_2$X$_2$ (R = Ph, Cy; X = Cl, Br),[32] [Os(≡N)X$_4$]$^-$,[33,34] Mo(≡N)-(depe)$_2$(N$_3$) (depe = 1,2-bis(diethylphosphino)ethane),[35] and [Mo(≡O)L$_4$]$^+$ (L = CNBu^t, 1/2 dmpe).[36] These compounds possess (d$_{xy}$)^2 ground states and (d$_{xy}$)^1(π*(ME))^1 excited states analogous to those of **1** and **1***, respectively; thus, the formal ME bond order is also reduced from 3.0 to 2.5 in the excited state. Franck−Condon analyses of the vibronically structured ^{1}[d$_{xy}$ → π*(ME)] electronic-absorption bands and ^{3}[d$_{xy}$ ← π*(ME)] luminescence bands of these compounds indicate that their M−E bonds are longer by 0.09−0.12 Å in the (d$_{xy}$)^1(π*(ME))^1 excited state relative to the ground state. These excited-state distortions are substantially larger than that found for **1***. The smaller distortion for **1*** is a consequence of extended π conjugation within the W≡CPh unit, which considerably lessens the local W≡C π antibonding character of the π*(WCPh) orbital relative to that of π*(ME) orbitals. This hypothesis could be tested by determination of the excited-state structure of a metal−alkylidyne complex possessing a saturated alkylidyne R group, although the observation of luminescence from such derivatives is, to date, relatively uncommon.[1]

One additional observation of note is that the W−C, W−P, and W−Cl bond distances of **1**, **1**$^+$, and **1*** are similar to each other. Although the inner-sphere reorganization energies for ground-state and excited-state electron transfer have not been determined for **1** or for other metal−alkylidyne compounds, it may be inferred from the structural data that these energies are small.

■ ASSOCIATED CONTENT

Ⓢ Supporting Information

X-ray crystallographic data for **1**·CH$_2$Cl$_2$, [**1**][OTf]·2CH$_2$Cl$_2$, and [**2**][BPh$_4$]·CH$_3$CN·Et$_2$O in CIF format; atomic coordinates from density-functional theory calculations of **1** and **1***; atomic parentage analysis of frontier orbitals; EPR spectrum of [**1**][OTf]; electronic-absorption spectra of [**1**][OTf] and [**2**][BPh$_4$]; ground-state XAS data for **1**; theoretical fits and fitting parameters for ground-state and excited-state XAS data for **1** and **1***. This material is available free of charge via the Internet at http://pubs.acs.org.

■ AUTHOR INFORMATION

Corresponding Author

*E-mail: mhopkins@uchicago.edu (M.D.H.), lchen@anl.gov (L.X.C.).

Present Addresses

$^\perp$Department of Chemistry, Wheaton College, Wheaton, IL $^\parallel$60187.

$^\parallel$Department of Chemistry, Rutgers University−Newark, Newark, NJ 07102.

$^\otimes$Advanced Nuclear Technology Group, N-2, MS B228, Los Alamos National Laboratory, Los Alamos, NM 87545.

$^\bigcirc$Department of Chemistry, Northwestern University, 2145 Sheridan Road, Evanston, IL 60208.

Notes

The authors declare no competing financial interest.

■ ACKNOWLEDGMENTS

We thank Dr. Ian Steele for performing the X-ray crystallography studies, Dr. Tony Marino of Prof. Jim Norris'

group for measuring the EPR spectrum, Dan O'Hanlon for assistance with some of the DFT calculations, and Prof. Richard Dallinger for measuring the emission lifetime. Research at the University of Chicago was supported by the U.S. Department of Energy, Office of Basic Energy Sciences, Solar Photochemistry Program (Grant DE-FG02-07-ER15910). Research at Argonne National Laboratory in the Chemical Sciences and Engineering Division was supported by the U.S. Department of Energy, Office of Science, Office of Basic Energy Sciences, under Contract DE-AC02-06CH11357. Work at the Argonne National Laboratory Advanced Photon Source was supported by the U.S. Department of Energy, Office of Science, Office of Basic Energy Sciences, under Contract DE-AC02-06CH11357. Experiments at the Advanced Photon Source were conducted during a time allocation provided by APS GUP-12007. S.Y. thanks the NSF MRSEC Program (Grant DMR-0820054), the University of Chicago–Argonne National Laboratory Joint Theory Institute, and the University of Chicago Energy Initiative for support.

REFERENCES

(1) Da Re, R. E.; Hopkins, M. D. *Coord. Chem. Rev.* **2005**, *249*, 1396.
(2) Bocarsly, A. B.; Cameron, R. E.; Rubin, H.-D.; McDermott, G. A.; Wolff, C. R.; Mayr, A. *Inorg. Chem.* **1985**, *24*, 3976.
(3) Bocarsly, A. B.; Cameron, R. E.; Mayr, A.; McDermott, G. A. In *Photochemistry and Photophysics of Coordination Compounds*; Yersin, H., Vogler, A., Eds.; Springer-Verlag: Berlin, Germany, 1987.
(4) Carter, J. D.; Kingsbury, K. B.; Wilde, A.; Schoch, T. K.; Leep, C. J.; Pham, E. K.; McElwee-White, L. *J. Am. Chem. Soc.* **1991**, *113*, 2947.
(5) Pollagi, T. P.; Geib, S. J.; Hopkins, M. D. *J. Am. Chem. Soc.* **1994**, *116*, 6051.
(6) Trammell, S.; Sullivan, B. P.; Hodges, L. M.; Harman, W. D.; Smith, S. R.; Thorp, H. H. *Inorg. Chem.* **1995**, *34*, 2791.
(7) Schoch, T. K.; Main, A. D.; Burton, R. D.; Lucia, L. A.; Robinson, E. A.; Schanze, K. S.; McElwee-White, L. *Inorg. Chem.* **1996**, *35*, 7769.
(8) Xue, W. M.; Wang, Y.; Mak, T. C. W.; Che, C. M. *J. Chem. Soc., Dalton Trans.* **1996**, 2827.
(9) Xue, W. M.; Chan, M. C. W.; Mak, T. C. W.; Che, C. M. *Inorg. Chem.* **1997**, *36*, 6437.
(10) Lee, F. W.; Chan, M. C. W.; Cheung, K. K.; Che, C. M. *J. Organomet. Chem.* **1998**, *552*, 255.
(11) Lee, F. W.; Chan, M. C. W.; Cheung, K. K.; Che, C. M. *J. Organomet. Chem.* **1998**, *563*, 191.
(12) Xue, W. M.; Wang, Y.; Chan, M. C. W.; Su, Z. M.; Cheung, K. K.; Che, C. M. *Organometallics* **1998**, *17*, 1946.
(13) Cavalheiro, C. C. S.; Torraca, K. E.; Schanze, K. S.; McElwee-White, L. *Inorg. Chem.* **1999**, *38*, 3254.
(14) Mayr, A.; Yu, M. P. Y; Yam, V. W. W. *J. Am. Chem. Soc.* **1999**, *121*, 1760.
(15) Lai, S.-W.; Chan, M. C. W.; Wang, Y.; Lam, H.-W.; Peng, S.-M.; Che, C. M. *J. Organomet. Chem.* **2001**, *617–618*, 133.
(16) Simpson, C. K.; Da Re, R. E.; Pollagi, T. P.; Steele, I. M.; Dallinger, R. F.; Hopkins, M. D. *Inorg. Chim. Acta* **2003**, *345*, 309.
(17) Jelliss, P. A.; Wampler, K. M. *Organometallics* **2005**, *24*, 707.
(18) Yu, M. P. Y; Yam, V. W. W.; Cheung, K. K.; Mayr, A. *J. Organomet. Chem.* **2006**, *691*, 4514.
(19) Cohen, B. W.; Lovaasen, B. M.; Simpson, C. K.; Cummings, S. D.; Dallinger, R. F.; Hopkins, M. D. *Inorg. Chem.* **2010**, *49*, 5777.
(20) Manna, J.; Geib, S. J.; Hopkins, M. D. *J. Am. Chem. Soc.* **1992**, *114*, 9199.
(21) Sun, J.; Shaner, S. E.; Jones, M. K.; O'Hanlon, D. C.; Mugridge, J. S.; Hopkins, M. D. *Inorg. Chem.* **2010**, *49*, 1687.
(22) Mayr, A.; Yu, M. P. Y *J. Organomet. Chem.* **1999**, *577*, 223.
(23) Semenov, S. N.; Blacque, O.; Fox, T.; Venkatesan, K.; Berke, H. *J. Am. Chem. Soc.* **2010**, *132*, 3115.
(24) Vogler, A.; Kisslinger, J.; Roper, W. R. *Z. Naturforsch.* **1983**, *38b*, 1506.
(25) Chen, L. X.; Zhang, X. Y.; Wasinger, E. C.; Attenkofer, K.; Jennings, G.; Muresan, A. Z.; Lindsey, J. S. *J. Am. Chem. Soc.* **2007**, *129*, 9616.
(26) Chen, L. X. *Annu. Rev. Phys. Chem.* **2005**, *56*, 221.
(27) Chen, L. X.; Shaw, G. B.; Liu, T.; Jennings, G.; Attenkofer, K. *Chem. Phys.* **2004**, *299*, 215.
(28) Chen, L. X. *Angew. Chem., Int. Ed.* **2004**, *43*, 2886.
(29) Chen, L. X.; Shaw, G. B.; Novozhilova, I.; Liu, T.; Jennings, G.; Attenkofer, K.; Meyer, G. J.; Coppens, P. *J. Am. Chem. Soc.* **2003**, *125*, 7022.
(30) Chen, L. X.; Jager, W. J. H.; Jennings, G.; Gosztola, D. J.; Munkholm, A.; Hessler, J. P. *Science* **2001**, *292*, 262.
(31) Miskowski, V. M.; Gray, H. B.; Hopkins, M. D. *Adv. Trans. Met. Coord. Chem.* **1996**, *1*, 159.
(32) Bailey, S. E.; Eikey, R. A.; Abu-Omar, M. M.; Zink, J. I. *Inorg. Chem.* **2002**, *41*, 1755.
(33) Cowman, C. D.; Trogler, W. C.; Mann, K. R.; Poon, C. K.; Gray, H. B. *Inorg. Chem.* **1976**, *15*, 1747.
(34) Hopkins, M. D.; Miskowski, V. M.; Gray, H. B. *J. Am. Chem. Soc.* **1986**, *108*, 6908.
(35) Mersmann, K.; Hauser, A.; Lehnert, N.; Tuczek, F. *Inorg. Chem.* **2006**, *45*, 5044.
(36) Da Re, R. E.; Hopkins, M. D. *Inorg. Chem.* **2002**, *41*, 6973.
(37) Pangborn, A. B.; Giardello, M. A.; Grubbs, R. H.; Rosen, R. K.; Timmers, F. J. *Organometallics* **1996**, *15*, 1518.
(38) Sun, J.; Simpson, C. K.; Hopkins, M. D. *Inorg. Synth.*, in press.
(39) Parker, C. A.; Rees, W. T. *Analyst* **1960**, *85*, 587.
(40) Suzuki, K.; Kobayashi, A.; Kaneko, S.; Takehira, K.; Yoshihara, T.; Ishida, H.; Shiina, Y.; Oishic, S.; Tobita, S. *Phys. Chem. Chem. Phys.* **2009**, *11*, 9850.
(41) Caspar, J. V.; Meyer, T. J. *J. Am. Chem. Soc.* **1983**, *105*, 5583.
(42) Sheldrick, G. *Acta Crystallogr.* **2008**, *A64*, 112.
(43) Lytle, F. W.; Sayers, D. E.; Stern, E. A. *Phys. Rev. B* **1975**, *11*, 4825.
(44) Stern, E. A.; Sayers, D. E.; Lytle, F. W. *Phys. Rev. B* **1975**, *11*, 4836.
(45) Sayers, D. E.; Stern, E. A.; Lytle, F. W. *Phys. Rev. Lett.* **1971**, *27*, 1204.
(46) Sayers, D. E.; Lytle, F. W.; Weissbluth, M.; Pianetta, P. *J. Chem. Phys.* **1975**, *62*, 2514.
(47) Oday, P. A.; Rehr, J. J.; Zabinsky, S. I.; Brown, G. E. *J. Am. Chem. Soc.* **1994**, *116*, 2938.
(48) Ankudinov, A.; Rehr, J. J. *Phys. Rev. B* **1995**, *51*, 1282.
(49) Newville, M.; Ravel, B.; Haskel, D.; Rehr, J. J.; Stern, E. A.; Yacoby, Y. *Phys. B (Amsterdam, Neth.)* **1995**, *209*, 154.
(50) Zabinsky, S. I.; Rehr, J. J.; Ankudinov, A.; Albers, R. C.; Eller, M. J. *Phys. Rev. B* **1995**, *52*, 2995.
(51) Ankudinov, A. L.; Ravel, B.; Rehr, J. J.; Conradson, S. D. *Phys. Rev. B* **1998**, *58*, 7565.
(52) Lavrentyev, A. A.; Nikiforov, I. Y.; Dubeiko, V. A.; Gabrelian, B. V.; Rehr, J. J. *J. Synchrotron Radiat.* **2001**, *8*, 288.
(53) Rehr, J. J.; Schattke, W.; de Abajo, F. J. G.; Muino, R. D.; Van Hove, M. A. *J. Electron Spectrosc. Relat. Phenom.* **2002**, *126*, 67.
(54) Frisch, M. J.; Trucks, G. W.; Schlegel, H. B.; Scuseria, G. E.; Robb, M. A.; Cheeseman, J. R.; Scalmani, G.; Barone, V.; Mennucci, B.; Petersson, G. A.; Nakatsuji, H.; Caricato, M.; Li, X.; Hratchian, H. P.; Izmaylov, A. F.; Bloino, J.; Zheng, G.; Sonnenberg, J. L.; Hada, M.; Ehara, M.; Toyota, K.; Fukuda, R.; Hasegawa, J.; Ishida, M.; Nakajima, T.; Honda, Y.; Kitao, O.; Nakai, H.; Vreven, T.; Montgomery, Jr., J. A.; Peralta, J. E.; Ogliaro, F.; Bearpark, M.; Heyd, J. J.' Brothers, E.; Kudin, K. N.; Staroverov, V. N.; Kobayashi, R.; Normand, J.; Raghavachari, K.; Rendell, A.; Burant, J. C.; Iyengar, S. S.; Tomasi, J.;. Cossi, M.; Rega, Millam, N. J.; Klene, M.;. Knox, J. E.; Cross, J. B.; Bakken, V.; Adamo, C.; Jaramillo, J.; Gomperts, R. E.; Stratmann, O.; Yazyev, A. J.; Austin, R.; Cammi, C.; Pomelli, J. W.; Ochterski, R.; Martin, R. L.; Morokuma, K.; Zakrzewski, V. G.; Voth, G. A.; Salvador, P.; Dannenberg, J. J.; Dapprich, S.; Daniels, A. D.; Farkas, O.; Foresman, J. B.; Ortiz, J. V.; Cioslowski, J.; Fox, D. J. *Gaussian 09*, Revision A.2; Gaussian, Inc.: Wallingford, CT, 2009.

(55) Perdew, J. P. *Phys. Rev. B* **1986**, *33*, 8822.
(56) Becke, A. D. *J. Chem. Phys.* **1993**, *98*, 5648.
(57) Bühl, M.; Reimann, C.; Pantazis, D. A.; Bredow, T.; Neese, F. *J. Chem. Theory Comput.* **2008**, *4*, 1449.
(58) Waller, M. P.; Braun, H.; Hojdis, N.; Bühl, M. *J. Chem. Theory Comput.* **2007**, *3*, 2234.
(59) Hay, P. J.; Wadt, W. R. *J. Chem. Phys.* **1985**, *82*, 299.
(60) Ehlers, A. W.; Bohme, M.; Dapprich, S.; Gobbi, A.; Hollwarth, A.; Jonas, V.; Kohler, K. F.; Stegmann, R.; Veldkamp, A.; Frenking, G. *Chem. Phys. Lett.* **1993**, *208*, 111.
(61) Dunning, T. H., Jr.; Hay, P. J. In *Methods of Electronic Structure Theory*; Schaefer, H. F., III, Ed.; Plenum Press: New York, 1977; Vol. 2.
(62) Magnusson, E.; Schaefer, H. F. *J. Chem. Phys.* **1985**, *83*, 5721.
(63) Andrae, D.; Häußermann, U.; Dolg, M.; Stoll, H.; Preuß, H. *Theoret. Chim. Acta* **1990**, *77*, 123.
(64) Martin, J. M. L.; Sundermann, A. *J. Chem. Phys.* **2001**, *114*, 3408.
(65) Kendall, R. A.; Dunning, T. H. Jr.; Harrison, R. J. *J. Chem. Phys.* **1992**, *96*, 6796.
(66) Gorelsky, S. I. *AOMix*, version 6.36; Department of Chemistry, York University: Toronto, Canada, 2010; http://www.sg-chem.net.
(67) Glendening, E. D.; Badenhoop, J. K.; Reed, A. E.; Carpenter, J. E.; Bohmann, J. A.; Morales, C. M.; Weinhold, F. *NBO*, version 5.9; Theoretical Chemistry Institute, University of Wisconsin: Madison, WI, 2001.
(68) Thompson, M. A. *Arguslab*, version 4.01; Planaria Software LLC: Seattle, WA; http://www.arguslab.com.
(69) The TD-DFT calculation also predicts two closely spaced electronic transitions that possess substantial π(WCPh) → π^*(WCPh) character, lying at 351 nm (36% 248a → 250a) and 364 nm (39% 248a → 250a). The oscillator strengths of these two transitions are the strongest among all predicted transitions in the region below 330 nm.
(70) Atagi, L. M.; Mayer, J. M. *Polyhedron* **1995**, *14*, 113.
(71) Churchill, M. R.; Rheingold, A. L.; Wasserman, H. J. *Inorg. Chem.* **1981**, *20*, 3392.
(72) Manna, J.; Gilbert, T. M.; Dallinger, R. F.; Geib, S. J.; Hopkins, M. D. *J. Am. Chem. Soc.* **1992**, *114*, 5870.
(73) Menoret, C.; Spasojevic-de Bire, A.; Dao, N. Q.; Cousson, A.; Kiat, J. M.; Manna, J. D.; Hopkins, M. D. *J. Chem. Soc., Dalton Trans.* **2002**, 3731.
(74) van der Eide, E. F.; Piers, W. E.; Parvez, M.; McDonald, R. *Inorg. Chem.* **2007**, *46*, 14.
(75) Furno, F.; Fox, T.; Schmalle, H. W.; Berke, H. *Organometallics* **2000**, *19*, 3620.
(76) Zou, F. L.; Furno, F.; Fox, T.; Schmalle, H. W.; Berke, H.; Eckert, J.; Chowdhury, Z.; Burger, P. *J. Am. Chem. Soc.* **2007**, *129*, 7195.
(77) John, K. D.; Hopkins, M. D. *Chem. Commun.* **1999**, 589.
(78) Manna, J.; Geib, S. J.; Hopkins, M. D. *Angew. Chem., Int. Ed. Engl.* **1993**, *32*, 858.
(79) Manna, J.; Mlinar, L. A.; Kuk, R. J.; Dallinger, R. F.; Geib, S. J.; Hopkins, M. D. In *Transition Metal Carbyne Complexes*; Kreissl, F. R., Ed.; Kluwer Academic Publishers: Dordrecht, The Netherlands, 1992; p 75.
(80) For a discussion of structural distortions in *trans*-M(E)$(dppe)_2$X compounds, see: Bendix, J.; Bogevig, A. *Inorg. Chem.* **1998**, *37*, 5992.
(81) It might be expected that the P−C bonds within the dppe ligands of **1** and $\mathbf{2}^+$ will be longer than those of $\mathbf{1}^+$, given the σ^*(P−C) character of the π-accepting dppe orbitals (Orpen, A. G.; Connelly, N. G. *Organometallics* **1990**, *9*, 1206) but because of the scatter in P−C distances within a given compound (ca. 0.02 Å) the observed differences are not statistically significant.
(82) Shannon, R. D. *Acta Crystallogr. A* **1976**, *32*, 751.
(83) The exceptions to the close agreement between calculated and observed metrical data are the C≡W−P angles. This is most likely due to the influence on the experimentally measured values of crystal packing forces, which are not modeled in the calculated (gas-phase) structure. Although calculated and observed average C≡W−P angles differ by <1°, the individual C≡W−P angles span a wider range in the calculated structure (87.6−102.2°) than the crystal structure (90.0−94.6°). This bending potential is expected to be soft and particularly susceptible to steric forces; a vibrational-spectroscopic study of the compound W(CH)$(PMe_3)_4$Cl and its isotopomers assigned a mode attributable to deformation of the WCP_4Cl subunit in the ca. 100 cm^{-1} region (Manna, J.; Dallinger, R. F.; Miskowski, V. M.; Hopkins, M. D. *J. Phys. Chem. B* **2000**, *104*, 10928). Consistent with this interpretation is the observation that the electronically similar d^2 compound $\mathbf{2}^+$ exhibits a much wider range of C≡W−P bond angles (89.7−99.9°) than does **1** (Table 3). The fact that the range of C≡W−P bond angles for $\mathbf{2}^+$ is similar to that calculated for **1** suggests that the difference between calculated and observed C≡W−P angles for **1** is within chemically reasonable limits..
(84) Pugliesi, I.; Tonge, N. M.; Hornsby, K. E.; Cockett, M. C. R.; Watkins, M. J. *Phys. Chem. Chem. Phys.* **2007**, *9*, 5436.
(85) Jacobsen, H.; Berke, H. *J. Chem. Soc., Dalton Trans.* **2002**, 3117.